Biology of Reproduction, 2022, **107(6)**, 1477–1489
https://doi.org/10.1093/biolre/ioac179
Advance access publication date 20 September 2022
Research Article

Morphogenesis of the female reproductive tract along antero-posterior and dorso-ventral axes is dependent on *Amhr2*+ mesenchyme in mice[1]

Shuai Jia[1], Jillian Wilbourne[1], McKenna J. Crossen[1,2] and Fei Zhao[1,2,*]

[1]Department of Comparative Biosciences, School of Veterinary Medicine, University of Wisconsin-Madison, Madison, WI, USA
[2]Endocrinology and Reproductive Physiology Program, University of Wisconsin-Madison, Madison, WI, USA

***Correspondence:** Department of Comparative Biosciences, School of Veterinary Medicine, University of Wisconsin-Madison, Madison, WI 53706, USA. Tel: +1-608-890-2610; E-mail: fei.zhao@wisc.edu

[†]**Grant support:** National Institute of Child Health and Development (R00-HD096051 to F.Z.).

Abstract

Morphogenesis of the female reproductive tract is regulated by the mesenchyme. However, the identity of the mesenchymal lineage that directs the morphogenesis of the female reproductive tract has not been determined. Using in vivo genetic cell ablation, we identified *Amhr2*+ mesenchyme as an essential mesenchymal population in patterning the female reproductive tract. After partial ablation of *Amhr2*+ mesenchymal cells, the oviduct failed to develop its characteristic coiling due to decreased epithelial proliferation and tubule elongation during development. The uterus displayed a reduction in size and showed decreased cellular proliferation in both epithelial and mesenchymal compartments. More importantly, in the uterus, partial ablation of *Amhr2*+ mesenchyme caused abnormal lumen shape and altered the direction of its long axis from the dorsal-ventral axis to the left–right axis (i.e., perpendicular to the dorsal-ventral axis). Despite these morphological defects, epithelia underwent normal differentiation into secretory and ciliated cells in the oviduct and glandular epithelial cells in the uterus. These results demonstrated that *Amhr2*+ mesenchyme can direct female reproductive tract morphogenesis by regulating epithelial proliferation and lumen shape without affecting the differentiation of epithelial cell types.

Summary Sentence

Amhr2+ mesenchyme regulates morphogenesis of the female reproductive tract along antero-posterior and dorso-ventral axes.

Keywords: Amhr2, antero-posterior axis, dorso-ventral axis, Müllerian duct, mesenchyme, morphogenesis

Introduction

Establishment of the female reproductive tract organs requires proper morphogenesis of the Müllerian duct, the progenitor for the epithelium of the entire female reproductive tract organs. Along the antero-posterior (i.e., rostral-caudal) axis, the Müllerian duct gives rise to structurally and functionally unique organs including the coiled oviduct, the straight uterus, cervix and the upper vagina [1, 2]. Classic tissue recombination studies have demonstrated that organ-specific mesenchymal signaling dictates the regionalization of the female reproductive tract along the antero-posterior axis. For instance, tissue recombinants consisting of uterine mesenchyme and vaginal epithelium displayed uterine morphology, while the tissue recombinants consisting of vaginal mesenchyme and uterine epithelium underwent vaginal morphogenesis [3]. The female reproductive tract, particularly the uterus, is also patterned along the dorso-ventral axis (also known as the mesometrial–anti-mesometrial axis) [4]. The uterine epithelial lumen is elongated along the dorsal-ventral axis at birth and forms differential structures at the dorsal and ventral sides. Epithelia at the dorsal (mesometrial) side develop the uterine rail, a morphological structure similar to a railroad track along the dorsal pole [5]. On the other hand, at the ventral (anti-mesometrial) side, luminal epithelium forms the ventral ridge, a continuous and smooth longitudinal epithelial invagination into the surrounding mesenchyme to establish uterine glands [6]. As a result, uterine gland formation is absent on the dorsal side and only occur at the ventral region [7]. The differential establishment of uterine glands along the dorso-ventral axis is regulated by differential mesenchymal WNT signaling. Active Wnt signaling that is essential for uterine gland formation is inhibited by the Wnt inhibitor *Dkk2* derived specifically from the dorsal mesenchyme [8]. These observations show that patterning of female reproductive tract organs along both the antero-posterior and dorso-ventral axes is governed by the mesenchyme.

AMHR2 (anti-Müllerian hormone receptor type II) is the specific receptor for mediating the action of anti-Müllerian hormone (AMH), a member of the transforming growth factor beta gene family [1]. *Amhr2* is specifically expressed in Müllerian duct mesenchyme in both male and female embryos around E12.5–E13 [9, 10]. In male embryos, AMHR2 is activated by testis-derived AMH to induce Müllerian duct regression via mesenchymal–epithelial interaction [9, 10]. On the other hand, in female embryos, the ovary does not produce AMH; as a result, AMHR2-mediated pathway remains inactive, and the Müllerian duct is maintained. Despite the lack of the ligand activation, *Amhr2* expression is still present and displays dynamic pattern in the mesenchyme in females. *Amhr2* is predominantly expressed in the prospective ventral

Received: May 9, 2022. **Revised:** August 11, 2022. **Accepted:** September 15, 2022

(anti-mesometrial) mesenchyme at the fetal stage and becomes restricted to a thin layer of subluminal mesenchyme in the uterus after birth before PND6. When the myometrium is formed from PND6 onwards, its expression is detected only in the circular smooth muscle layer [10, 11]. When *Amhr2* promoter driven Cre (*Amhr2-Cre*) was generated and crossed with a reporter, the majority of mesenchymal cells in the oviduct and uterus were labeled starting from E12.5 [9, 12]. Therefore, *Amhr2-Cre* has been widely used to study functions of the mesenchymal factors in female reproductive tract biology. As reported in previous literature, deletion of either *Tgfbr1* or *Tbfbr2* in *Amhr2+* mesenchyme caused oviductal diverticula, myometrial defects, and endometrial hyperplasia [13, 14]. Ablations of the key Hippo kinases *Lats1* and *Lats2* in the *Amhr2+* mesenchyme led to profound developmental defects, including cystic oviducts, shortened uterine horns, and the absence of uterine glands [15].

Targeting a couple of genes at a time does not reveal the comprehensive role of *Amhr2+* mesenchyme in female reproductive tract development. A powerful way to elucidate the function of a specific cell population within the whole organism is in vivo genetic cell ablation using the *Rosa-DTA* (diphtheria toxin fragment A) mouse line. Upon Cre-mediated excision of the *loxP*-flanked transcriptional stop sequence, DTA expression is induced specifically in Cre-expressed cells, where DTA induces cell apoptosis by inhibiting protein translation [16]. Because mice do not express the membrane receptor for the internalization of DTA, DTA released from the apoptotic cells cannot enter surrounding non-Cre-expressed cells, avoiding nonspecific cell ablation [16]. We therefore set out to use *Amhr2-Cre; Rosa-DTA* genetic cell ablation model to specifically ablate *Amhr2+* mesenchyme to reveal functional significances of *Amhr2+* mesenchyme in female reproductive tract development.

Materials and methods

Mice

Amhr2-Cre line was provided by Richard Behringer (The University of Texas MD Anderson Cancer Center) and maintained in C57BL/6 genetic background [17]. *Rosa-DTA* line (stock# 006331) was originally purchased from Jackson Laboratories (Bar Harbor, ME) and maintained with their original genetic background (C57BL/6 J and CD1). Timed mating was set up by housing stud males with two to three sexually mature females (2–6 months old) in the later afternoon. Vaginal plugs were checked early on the next morning, and the day of plug detection was designated as embryonic day 0.5 (E0.5). The day of birth was determined by examining pup delivery in the afternoon and was designated as postnatal day 0 (PND0). The embryos or mice harboring both $Amhr2^{Cre/+}$ and $Rosa^{DTA/+}$ were used in the ablation group while mice of other genotypes ($Amhr2^{Cre/+}$; $Rosa^{+/+}$, $Amhr2^{+/+}$; $Rosa^{DTA/+}$, or $Amhr2^{+/+}$; $Rosa^{+/+}$) were mixed as the control for morphological analyses and tissue section staining. All experiments were performed at least on three mice for each group and the number of mice used for each experiment was described in figure legends. All mouse procedures were approved by the University of Wisconsin-Madison (UW-Madison) Animal Care and Use Committees and are in compliance with UW-Madison approved animal study proposals and public laws.

Genotyping

PCR was performed with primers (Forward: 5′-CGCATTGT CTGAGTAGGTGT-3′, Reverse: 5′-GAAACGCAGCTCGGC CAGC-3′) for *Amhr2-Cre* allele [18] and primers (Mutant Reverse: 5′-GCGAAGAGTTTGTCCTCAACC-3′, Common: 5′-AAAGTCGCTCTGAGTTGTTAT-3′, Reverse: 5′-GGAGC GGGAGAAATGGATATG-3′) for *Rosa-DTA* allele. Platinum II Taq Hot-Start DNA Polymerase (Invitrogen, Catalog #: 14966001) was used to run the thermal cycle: 94 °C for 2 min, 34 cycles of [94 °C for 15 s, 60 °C for 5 s, and 68 °C for 15 s] followed by 68 °C for 5 min.

Tissue processing, embedding, and sectioning

Tissues were fixed in 10% neutral buffered formalin (Leica, Catalog #: 3800598) overnight at room temperature, washed three times with 1 × PBS for 10 min each, dehydrated by a serial of ethanol (70%, 80%, and 95% for 30 min for each; 100% ethanol I and II for 50 min for each), cleared (100% ethanol: xylene =1:1 for 5 min; xylene I for 5 min; xylene II for 3 min), and infiltrated with paraffin (100% ethanol: soft paraffin =1:1 for 0.5 h; soft paraffin I for 1.5 h; soft paraffin II for 1 h; soft paraffin: hard paraffin = 1:1 for 1 h; hard paraffin for 1.5 h) before being embedded in paraffin. Tissues were sectioned at 5 μm using a microtome (TN6000, Tanner Scientific) and were collected at least 50 μm apart from each other for subsequent immunofluorescence staining and quantifications.

H&E staining was performed as previously described [19]. Briefly, paraffin sections were deparaffinized, rehydrated, and stained with hematoxylin (Electron Microscopy Sciences, Catalog #: 26123-08). After hematoxylin staining, slides were rinsed in running tap water, decolorized in acid ethanol, rinsed in running tap water, and then counterstained with eosin (Leica Biosystems, Catalog #: 3801615). After counterstaining, sections were dehydrated with gradient ethanol, cleared in xylene, and mounted with mounting medium (Fisher Chemical, Catalog #: SP15500). All images were taken under a Nikon ECLIPSE E600 microscope.

Immunofluorescence

Paraffin sections were deparaffinized and rehydrated (the same as described in H&E staining). Sections were then subjected for antigen retrieval using a microwave oven (35PF91, Grainger) with commercial antigen unmasking solution (VECTOR, Catalog #: H-3300) and underwent immunostaining procedure using the Sequenza Immunostaining Center System (Electron Microscopy Sciences, Catalog #: 71407-01) [20]. Briefly, sections were washed with 1×PBS and PBST (1× PBS with 0.1% Triton X-100) and incubated with blocking solution (5% Donkey serum in PBST) for 1 h at room temperature and then with primary antibody in blocking solution overnight at 4 °C. After being washed three times in PBST, sections were incubated with secondary antibodies for 1 h at room temperature and counterstained by DAPI (1:1000, Thermo Scientific, Catalog #:62248), coverslipped with EverBrite mounting medium (Biotium, Catalog #: 23003) for imaging under a Leica TCS SP8 confocal microscope.

The following primary antibodies were used: rabbit anti-Cleaved PARP1 [E51] (1:300, Abcam, Catalog #: ab32064), rabbit anti-Ki67(1:300, Abcam, Catalog #: ab15580), rabbit anti-alpha-smooth muscle actin (αSMA) (1:200, Abcam,

Catalog #: ab5694), rabbit anti-FOXA2 [EPR4466] (1:200, Abcam, Catalog #: ab108422), rabbit anti-PAX8 polyclonal (1:200, Proteintech, Catalog #: 10336-1-AP), and mouse anti-β-Tubulin IV [Clone ONS1A6] (1:200, Biogenex, Catalog #: MU178). The secondary antibodies conjugated with different fluorescent dyes were used: donkey anti-rabbit IgG (H + L), Alexa Fluor 488 (1:200, Invitrogen, Catalog #: A-21206) and donkey anti-mouse IgG (H + L), Alexa Fluor 568 (1:200, Invitrogen, Catalog #: A-10037).

RNAscope

RNAscope was performed in formalin fixed paraffin embedded tissues using RNAscope 2.5 HD Detection Reagent according to the manufacturer's instructions (Advanced Cell Diagnostics, Newark, CA). Tissues were fixed in fresh 10% formalin for 24 h at the room temperature. After fixation, tissues were processed, embedded in paraffin, sectioned at 5 μm, deparaffinized, and rehydrated. Then sections were treated with antigen retrieval buffer and proteinase. Sections were exposed to Amhr2 (489821) probe and subjected to a series of rinsing and signaling detection. All sections were imaged under a compound microscope. Mesenchymal cells that had at least one signaling dot were counted as Amhr2+ cells.

Quantifications of cleaved-PARP1+ and Ki67+ cells

Images of three to seven sections from each of the five to seven mice were analyzed using ImageJ. For quantifying cleaved-PARP1+ cells, autofluorescent cells identified by imaging in another color channel were excluded [21]. For Ki67+ proliferating cells, only cells with over 50% of the nucleus exhibiting Ki67 positive staining were counted as cells in the active process of mitosis [22, 23]. To count Ki67+ cells in the mesenchymal compartment, images of uterine sections were divided into dorsal and ventral regions by drawing lines perpendicular to the dorso-ventral axis at the center of epithelial lumen. The total number of cells (DAPI staining for individual nucleus), cleaved-PARP1+ and Ki67+ cells in epithelial or mesenchymal compartments in each section, was counted twice and averaged. The percentage of apoptotic or proliferating cells was calculated as the fraction of cleaved-PARP1+ or Ki67+ cells over the total number of cells in each section for subsequent statistical analysis. Three independent examiners followed the same criteria and procedures for counting cells to confirm statistical differences.

Quantifications of FOXA2+ uterine glands

Images of three to five sections from PND21 uteri were analyzed using ImageJ.

Measurement of oviductal length and width

After removing connective tissues, the oviduct was placed on a membrane for image acquisition. In the image, a curve was artificially drawn at the center of the oviductal lumen from the distal end (the ostium) of infundibulum to the uterine-tubal junction (the flexura medialis on E16.5) [24]. ImageJ was used to measure the length of the curve twice and average the two measurements for each oviduct. Three independent examiners followed the same criteria and procedures to confirm statistical differences. For measuring oviductal width, three measurements at the head, middle, and tail regions of the ampulla and isthmus were averaged for each mouse.

Measurement of ovary size, uterine length, uterine width, and uterine stromal area

The same procedure for measuring oviductal parameters was used for the ovary and uterus. The uterine stromal area was defined as the region between myometrial and epithelial layers.

Measurement of muscle layer thickness

Three different regions at the anti-mesometrial side of a uterine section or at random regions of an oviductal section were measured and averaged. Images of three to five sections from each mouse were analyzed using ImageJ.

Statistical analyses

The significant differences between control and ablation groups were evaluated by two-tailed unpaired Student's t-test using GraphPad Prism 9.0 software. Results were shown as mean ± s.e.m. The significance level was set at $P < 0.05$.

Results

The number of apoptotic cells in the mesenchymal compartment was significantly increased in the *Amhr2-Cre; Rosa-DTA* female reproductive tract

The Cre activity of *Amhr2-Cre* initiates around E12.5 in the Müllerian duct mesenchyme [9]. It takes up to 48 h from the onset of Cre expression to the recombination of the *loxP*-flanked stop codon, allowing DTA expression and DTA-induced apoptosis [16, 25]. In addition, the antero-posterior regionalization of the Müllerian duct occurs around E16.5 [26–28]. We therefore examined the expression of apoptotic marker, cleaved Poly [ADP-ribose] polymerase 1 (PARP1), in E16.5 Müllerian ducts to determine whether our *Amhr2-Cre; Rosa-DTA* model successfully induced death of *Amhr2*+ mesenchymal cells [29] (Figure 1A–D). By correcting background autofluorescent cells, we found that less than 0.1% cells in mesenchymal compartment were positive for cleaved-PARP1 in the anterior (future oviduct, 0.02 ± 0.02%) and posterior (future uterus, 0.07 ± 0.06%) Müllerian ducts of the control group. On the contrary, percentages of cleaved-PARP1+ cells were significantly increased both in the anterior (0.34 ± 0.05%) and posterior regions (0.95 ± 0.12%) of the ablation group (Figure 1E). In addition, we also performed *Amhr2* RNAscope assays to identify Amhr2+ mesenchymal cells in both control and ablation uterus on PND0. We found that the number of Amhr2+ mesenchymal cells was significantly reduced to 41.9% of that in the control group on average (Supplementary Figure S1), which indicated the elimination efficiency. When *Amhr2-Cre* reporter lines were used to track *Amhr2*+ mesenchyme [9, 30], *Amhr2*+ mesenchymal cells contributed to the majority of mesenchymal cells in both oviducts and uteri. There are two possible explanations for the partial cell ablation: either cells escape recombination or recombination occurs but somehow cells do not express lethal amounts of DTA. These results demonstrate that the *Amhr2-Cre; Rosa-DTA* model successfully achieves partial ablation of *Amhr2*+ mesenchymal cells.

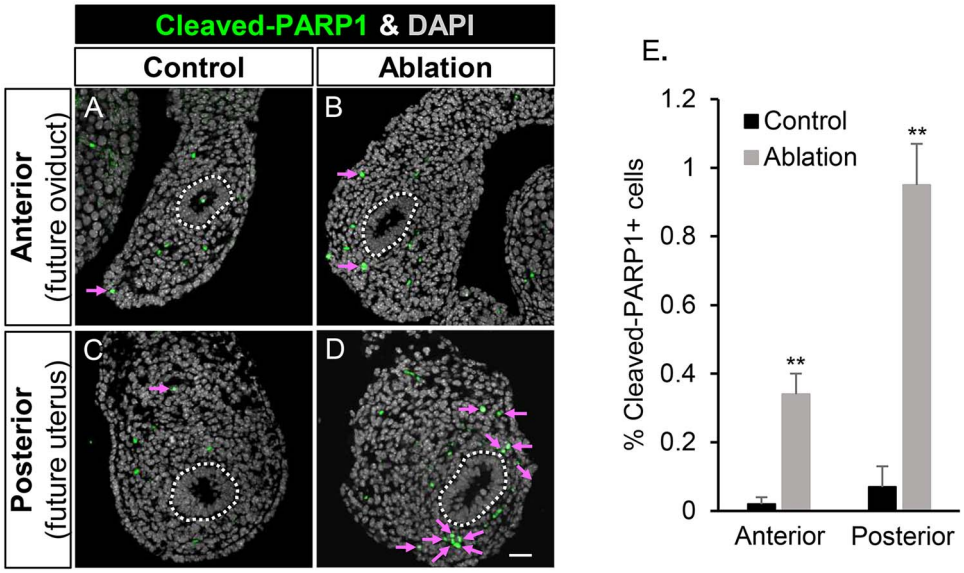

Figure 1. Increased apoptotic cells in the mesenchymal compartment of E16.5 Müllerian ducts in the ablation group. (A–D) Immunofluorescence staining of the apoptotic marker cleaved-PARP1 and DAPI for nuclei in the anterior and posterior regions of E16.5 Müllerian duct in the control (A and C) and ablation (B and D) groups. Pink arrows indicate identified apoptotic cells. Dashed lines: Müllerian ducts. (E) Percentages of apoptotic cells in the control and ablation groups. Results were shown as mean ± s.e.m. and analyzed by two-tailed unpaired Student's *t* test. **, $P < 0.01$ compared with the control group at the same age. $N = 3$ for each group. Scale bar: 25 μm.

Defective oviductal coiling but normal oviductal epithelial regionalization and differentiation in the ablation group

Next, we determined the consequence of partial ablation of *Amhr2*+ mesenchymal cells by examining gross morphology of the female reproductive tract on PND21, when the patterning of the female reproductive tract is complete [31]. The female reproductive tracts were smaller and shorter in the ablation group compared to those in the control group (Figure 2A). In the control group, the Müllerian duct differentiates into two morphologically distinct organs: the highly coiled oviduct in the anterior region and the straight uterus in the posterior region (Figure 2A). However, we found that the antero-posterior patterning was defective in the ablation group where the oviduct lost its characteristic coiling (Figure 2A). In addition to coiling formation, the oviduct undergoes regionalization and further differentiation into three morphologically and histologically distinct segments along the antero-posterior axis: the infundibulum that has the ostium (the opening) surrounded fimbriae (fingerlike epithelial projections); the ampulla that possess more longitudinal epithelial folds but thin smooth muscle layers; and the isthmus that has less epithelial folds but thicker smooth muscle layers [32] (Figure 2B). These three segments with their typical histological structures were observed in the uncoiled oviduct of the ablation group in both whole mount images and histological sections (Figure 2A and B). The observation of uncoiled oviducts with normal regionalization suggests that oviductal coiling and regionalization could be two uncoupled events.

Oviductal epithelium consists of two major cell types: ciliated and secretory epithelial cells [33]. To determine whether epithelial cell differentiation is impaired in the oviduct of the ablation group, we performed double-immunofluorescence staining of PAX8 (Paired box 8, a secretory epithelial cell marker) and TUBB4A (Tubulin beta 4A class IVa, a ciliated cell marker) to visualize both cell types. In the control group, PAX8 expression was detected in all three regions and its abundance was gradually increased from the infundibulum to the isthmus (Figure 2C and Supplementary Figure S2). On the other hand, TUBB4A+ ciliated cells were the most abundant in the epithelium of the infundibulum, and were decreased from the infundibulum to the isthmus (Figure 2C and Supplementary Figure S2). These results were consistent with other studies on the abundancy of ciliated and secretory cells from the infundibulum to the isthmus [34–36]. In the ablation group, both PAX8 and TUBB4A expression were detected in all three regions (Figure 2C) and their abundances along the antero-posterior axis were comparable with those in the control group (Supplementary Figure S2). These results demonstrated that the partial ablation of *Amhr2*+ mesenchymal cells leads to defective oviductal coiling without disrupting the normal epithelial regionalization and differentiation.

Defective ovarian development in the ablation group

Amhr2-Cre also targets somatic cells in the ovary as early as E17.5 [37]. We therefore determined whether ovarian development was affected from E16.5 to PND21. In the control group, ovaries were in oval shape and displayed follicles on the surface. In contrast, ovaries in the ablation group were irregular in shape and much smaller in size with few follicles on the surface (Figure 3A and B). Histological examination on PND21 revealed that the ovaries in the ablation group had normal follicular structure but contained fewer follicles (Figure 3C). These results demonstrate that ovarian and follicular development were impaired in our ablation model. However, it has been well established that ovaries do not play any significant roles in fetal and postnatal female reproductive tract development before PND25 [38–40]. Therefore, abnormal ovarian development would not contribute to the

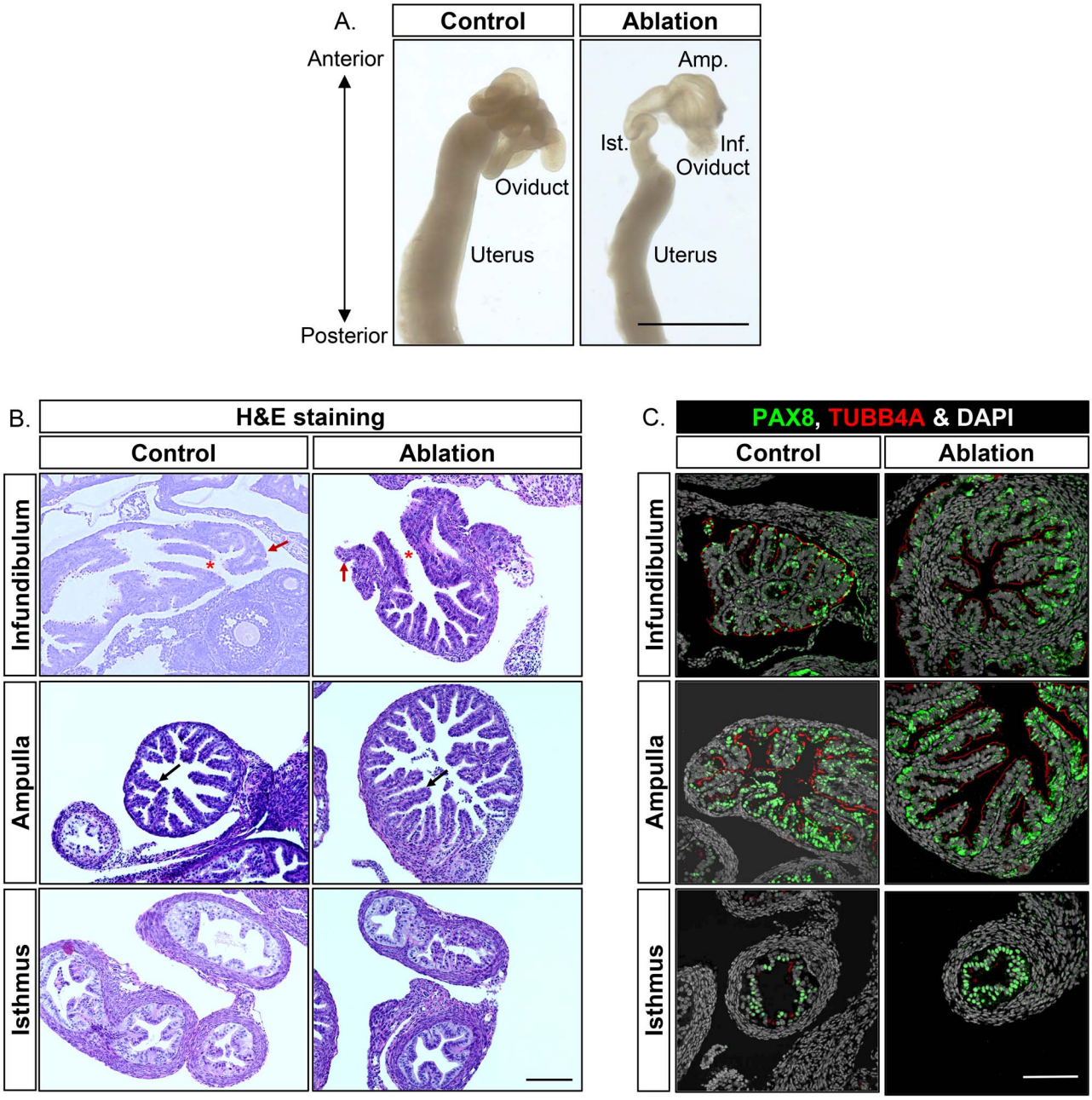

Figure 2. Defective oviductal coiling but normal epithelial regionalization and differentiation in the ablation group. (A) Representative images of PND21 oviducts and uteri of the control and ablation group. Scale bar: 2 mm. (B) Histology of PND21 oviducts and uteri of the control and ablation groups. Stars: ostium. Red and black arrows: fimbriae and epithelial folds, respectively. (C) Double immunofluorescence staining of the ciliated cell marker TUBB4A and secretory cell marker PAX8 in the infundibulum, ampulla, and isthmus. Scale bar: 100 μm in B and C. $N = 3$ for both the control and ablation groups for A, B, C.

phenotype of the female reproductive tract in our cell ablation model. We next focused on investigating cellular mechanisms of defective female reproductive tract development observed in the ablation group.

Impaired oviductal elongation during development in the ablation group

Coiling morphogenesis depends on the elongation and growth of tubular organs [41]. To determine whether oviductal elongation was affected during development, we measured the oviductal length from the distal end of the oviduct to the uterine-tubal junction and oviductal width over the course of the oviducal coiling (E16.5–PND15) [27]. In the control group, the oviduct was a straight tube on E16.5 and then became coiled with an increased number of turns and lengths starting from PND0 (E16.5: 4.23 ± 0.19 mm; PND0: 5.16 ± 0.13 mm; PND3: 7.04 ± 0.45 mm; PND7: 15.44 ± 1.46 mm; PND15: 20.17 ± 0.47 mm) (Figure 4A and B). On the contrary, in the ablation group, the oviduct remained uncoiled on all examined timepoints (Figure 4A). On E16.5 prior to the initiation of coiling on PND0, the length of oviductal region in the ablation group was already significantly shorter than those of the control group. From E16.5 to PND15,

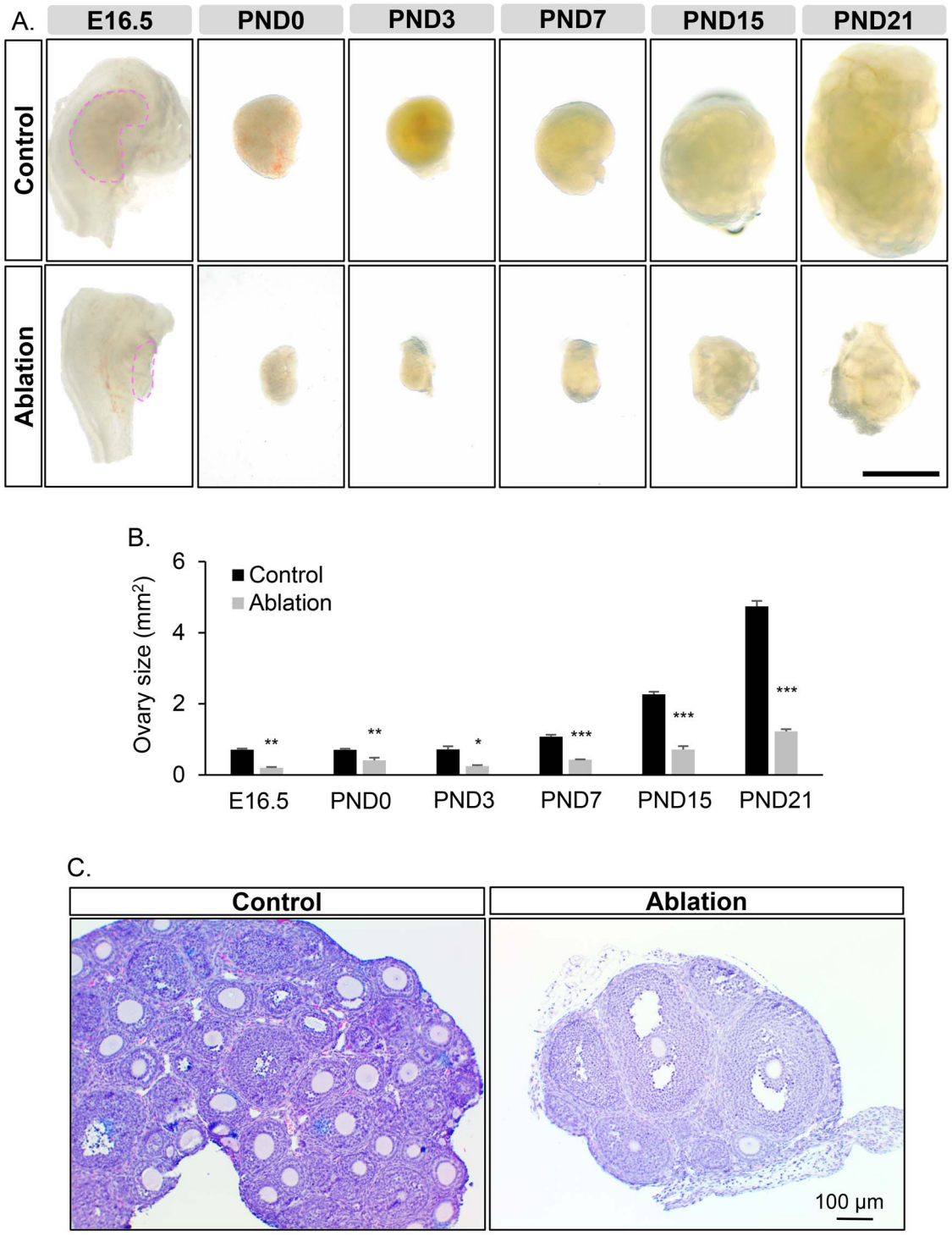

Figure 3. Impaired ovarian development in the ablation group. (A) Representative images of ovaries in the control and ablation groups from E16.5 to PND21. Scale bar: 1 mm. (B) Quantification of ovary size. $N = 5$ for control group and $N = 3$ for ablation group in E16.5 group; $N = 3$ for both control and ablation groups from PND0 to PND21. Results were shown as mean ± s.e.m. and analyzed by two-tailed unpaired Student's *t* test. *, $P < 0.05$; **, $P < 0.01$; ***, $P < 0.001$ compared with the control group at the same age. (C) Representative histology of the ovaries in the control and ablation group. $N = 5$ in each group. Scale bar: 100 μm.

the oviductal length in the ablation group was increased but remained 40–60% of their counterparts in the control group (E16.5: 2.49 ± 0.07 mm vs 4.23 ± 0.19 mm; PND0: 3.50 ± 0.40 mm vs 5.16 ± 0.13 mm; PND3: 3.71 ± 0.26 mm vs 7.04 ± 0.45 mm; PND7: 6.18 ± 0.79 mm vs 15.44 ± 1.46 mm; PND15: 7.06 ± 0.12 mm vs 20.17 ± 0.47 mm) (Figure 4B). The oviductal width was not changed in the ablation groups except for the ampulla region on PND3 (Figure 4C). These results demonstrate that the partial ablation of *Amhr2*+ mesenchymal cells impairs oviductal elongation during development, which contribute to defective oviductal coiling.

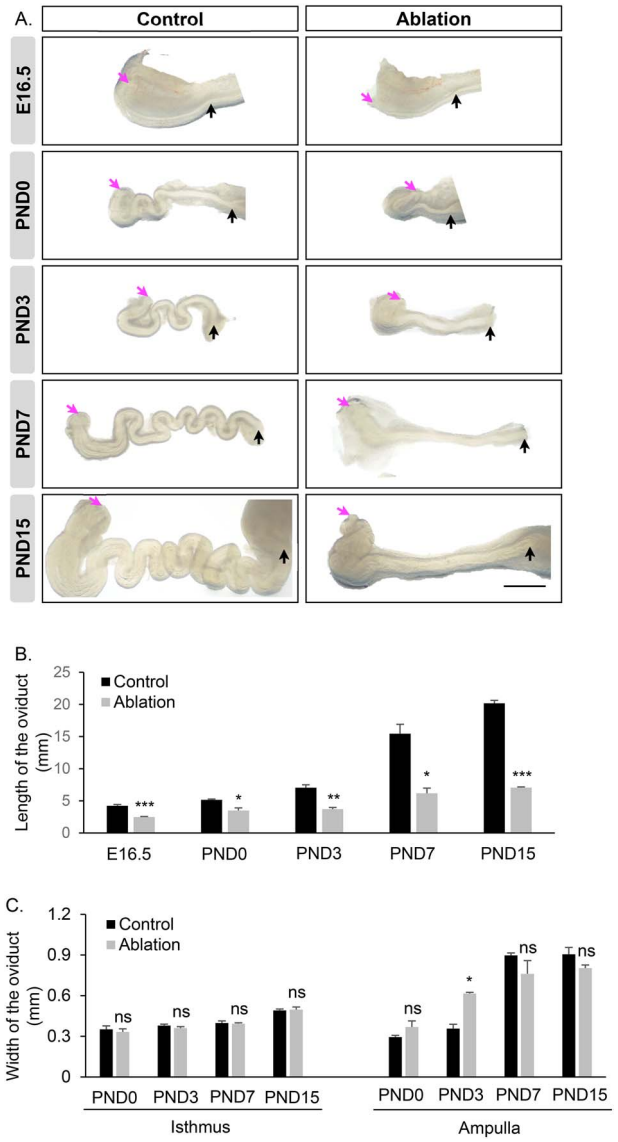

Figure 4. Impaired oviductal elongation during development in the ablation group. (A) Representative images of oviducts in the control and ablation groups from E16.5 to PND15. Scale bar: 1 mm. Pink and black arrows indicate the ostium of infundibulum and the uterine-tubal junction (the flexura medialis on E16.5), respectively. (B) Quantification of oviductal lengths in the control and ablation groups. $N = 3$–7. (C) Quantification of oviducal width in the isthmus and ampulla region. $N = 3$–4. Results were shown as mean ± s.e.m. and analyzed by two-tailed unpaired Student's *t* test. ns, $P > 0.05$, not significant; *, $P < 0.05$; **, $P < 0.01$; ***, $P < 0.001$; ****, $P < 0.0001$ compared with the control group at the same age.

Decreased proliferation in the oviductal epithelium in the ablation group

Epithelial proliferation has been implicated in tubular organ elongation [42]. Therefore, we performed immunofluorescence staining of the proliferating marker Ki67 (marker of proliferation Ki-67) to determine the percentage of Ki67+ proliferating cells in oviductal epithelia on PND0 when the oviductal elongation initiates (Figure 5A). In the control group, the percentage of Ki67+ cells was 30% on the average (Figure 5B), which was significantly decreased to 20% in the ablation group. These results demonstrate that the partial ablation of *Amhr2*+ mesenchymal cells significantly decreases oviductal epithelial proliferation.

Defective uterine elongation and growth in the ablation group

We next characterized the uterine phenotype by determining whether uterine elongation and growth was affected during development from E16.5 to PND21 (Figure 6A). The length of the uterine horn was significantly reduced in the ablation group on all time points examined (Figure 6B). The width of the uterus was comparable between the control and ablation group on E16.5, PND3, and PND7 but significantly decreased in the ablation group on PND0 and PND21 (Figure 6C). These results demonstrate that partial ablation of *Amhr2*+ mesenchyme leads to defective uterine elongation and growth.

Defective uterine patterning along the dorsal-ventral axis in the ablation group

To determine the consequence of partial ablation of *Amhr2*+ mesenchymal cells on uterine development, we examined uterine sections on PND0 and PND21, during which the epithelium undergoes extensive morphogenesis and forms uterine glands [43]. In the control group, uterine lumen was elongated along the dorsal-ventral axis on PND0, forming a flattened circle in the cross-section view (Figure 7A). The long axis of the uterine lumen remained along the dorsal-ventral axis on PND21 (Figure 7C). However, in the ablation group, lumen shape became irregular with its long axis perpendicular to the dorsal-ventral axis on both PND0 and PND21 (Figure 7B and D). However, on PND21, the mispatterning of the uterine shape was not observed in two of three mice examined (Figure 7D), suggesting that the misalignment of the uterine luminal shape can be resolved during postnatal development.

On PND21, the uterine epithelium extended into the stroma and established uterine glands at the lateral and ventral regions (Supplementary Figure S3A). In the ablation group, uterine glands were also observed in these two regions (Supplementary Figure S3A), and the number of uterine glands was decreased without significant differences (Supplementary Figure S3B). In addition, the area of uterine stromal layer was comparable between the control and ablation group (Supplementary Figure S3C). These results indicate that uterine gland formation and patterning was not affected in the ablation group.

Taken together, these results demonstrate that partial ablation of *Amhr2*+ mesenchymal cells does not affect uterine gland formation but disrupts the patterning of uterine epithelial lumen along the dorsal-ventral axis.

Decreased proliferation in epithelial and mesenchymal compartments of the uterus in the ablation group

We then performed immunostaining of the proliferating marker Ki67 to determine the percentage of Ki67+ proliferating cells in uterine epithelium and mesenchyme on PND0 when uterine defects were observed (Figure 8A). In the control group, average percentages of Ki67+ in epithelia and the whole mesenchyme were 26% and 27%, respectively (Figure 8B). However, the percentages were significantly decreased to 16% and 20% in the ablation group (Figure 8B). Given patterning of uterine lumen along the dorsal-ventral

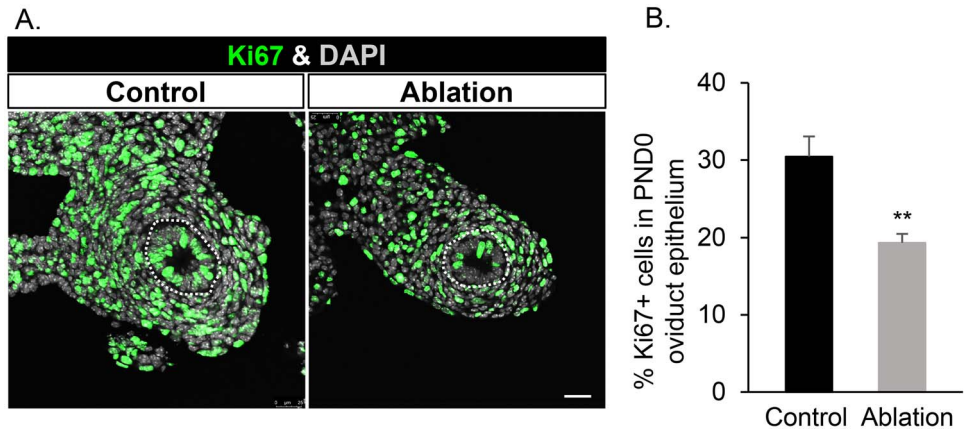

Figure 5. Decreased proliferation in the oviductal epithelium in the ablation group. (A) Representative images of Ki67 immunofluorescence staining on PND0 oviducts in the control and ablation groups. White dashed circles: oviductal epithelium. Scale bar: 25 μm. (B) Percentages of Ki67+ cells in the PND0 oviductal epithelia of the control and ablation groups. $N = 6, 5$ for the control and ablation group, respectively. Results were shown as mean ± s.e.m. and analyzed by two-tailed unpaired Student's t test. **, $P < 0.01$.

axis was altered, we then determined whether percentages of Ki67+ proliferating cells were differential in uterine dorsal and ventral mesenchyme. We found that percentages of Ki67+ proliferating cells in both dorsal and ventral regions were decreased but with statistical significance only observed in the dorsal mesenchymal compartments (Figure 8B, $P = 0.02$ on the dorsal side; $P = 0.07$ on the ventral side). These results demonstrate that partial ablation of *Amhr2*+ mesenchymal cells decreases cellular proliferation in both epithelial and mesenchymal compartments.

Normal smooth muscle formation in the oviduct but delayed smooth muscle formation at the dorsal side of the uterus in the ablation group

Smooth muscle formation is a key event of mesenchymal differentiation [44] and smooth muscles provide mechanical forces in tubular organ morphogenesis [45]. Therefore, we next investigated whether smooth muscle formation was affected in the ablation group by performing immunofluorescence staining of the smooth muscle marker αSMA on PND3 when smooth muscle cells initiate their differentiation [24, 27] and PND21 when both circular and longitudinal smooth muscle layers are formed [44]. In the oviduct, αSMA expression was detected in the inner circular layer of mesenchymal compartments in both anterior and posterior oviductal sections on PND3 (Figure 9A) and PND21 (Figure 9B) in both the control and ablation groups. In addition, the thickness of the αSMA stained smooth muscle layer in the oviduct was comparable between the control and ablation group on PND3 and PND21 (Figure 9D and E). These results demonstrate that partial ablation of *Amhr2*+ mesenchymal cells does not affect smooth muscle differentiation in the oviduct.

However, in the uterus, on PND3, in the control group, αSMA expression was detected in the circumferentially aligned (i.e., circular) smooth muscle cells of the uterus. (Figure 9C). However, in the ablation group, αSMA expression was absent in the dorsal part of the mesenchymal compartment and only formed a three-quarter circle of the smooth muscle layer (Figure 9C). On PND21, both the inner circular layer and the outer longitudinal layer of smooth muscles were visible in the uterus of both groups (Figure 9C). The thickness of the αSMA stained smooth muscle layer in the control and ablation uteri on PND3 and PND21 have no significant differences (Figure 9D and E). These results demonstrate that partial ablation of *Amhr2*+ mesenchymal cells delays the formation of circular smooth muscle in the dorsal region of the uterus.

Discussion

Our work reveals that the proper number of *Amhr2*+ mesenchymal cells is required for normal female reproductive tract patterning along both antero-posterior and dorso-ventral axes. Partial ablation of *Amhr2*+ mesenchyme compromises the oviductal coiling during antero-posterior patterning, alters uterine lumen shape, and delays smooth muscle formation in the dorsal-ventral axis.

Genetic cell ablation represents an important tool for advancing our understanding of female reproductive tract development

Genetic cell ablation technique has been used to discover significant roles of a specific cell type/lineage in development and function of other reproductive organs, including the testis [46–48] and ovary [49–51]. However, it has not been used in studying female reproductive tract development and function. Here, we used the *Amhr2-Cre; Rosa-DTA* genetic cell ablation model to reveal consequences of continuous ablation of *Amhr2*+ mesenchyme from the fetal stage on female reproductive tract differentiation. As far as we are concerned, among the phenotypes resulting from partial ablation of *Amhr2*+ mesenchyme, altered uterine lumen patterning and delayed smooth muscle formation have not been reported in any *Amhr2*-Cre driven gene knockouts. Therefore, *Rosa-DTA* model used in our study uncovers new roles of *Amhr2*+ mesenchyme in patterning the epithelial lumen and promoting smooth muscle differentiation. Multiple single cell RNA transcriptomic studies have identified mesenchymal subpopulations and their specific markers in the developing and adult uterus [11, 52, 53] and in the adult oviduct [35, 54]. With the availabilities of Cre or CreER under the control of marker gene promoters, subpopulation-specific cellular ablation studies can be feasible and potentially provide insights into their specific functions. These observations demonstrate that genetic cell ablation can provide comprehensive roles of

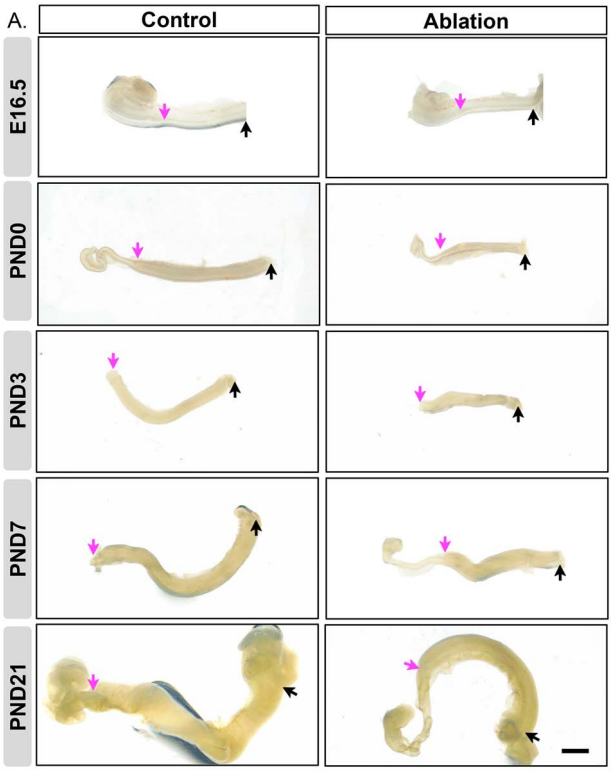

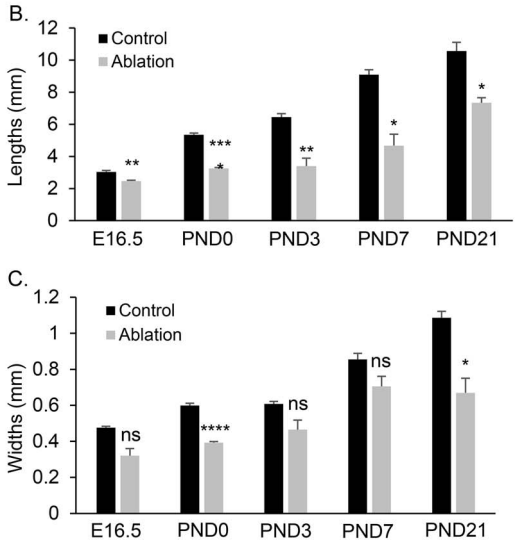

Figure 6. Defective uterine elongation and growth in the ablation group. (A) Representative images of uteri after fixation in the control and ablation group. Scale bar: 1 mm. Pink and black arrows indicate the uterine-tubal junction and uterine-cervical junction, respectively. (B) Quantification of uterine lengths in the control and ablation groups. $N = 3$–6. (C) Quantification of uterine width. $N = 3$–6. Results were shown as mean ± s.e.m. and analyzed by two-tailed unpaired Student's *t* test. ns, $P > 0.05$, not significant; *, $P < 0.05$; **, $P < 0.01$; ***, $P < 0.001$ compared with the control group at the same age.

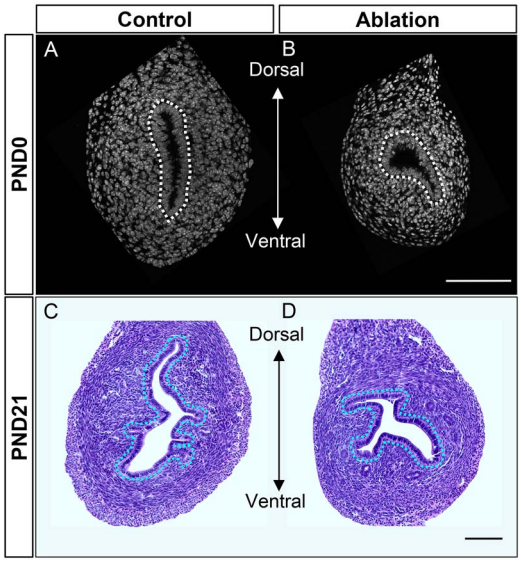

Figure 7. Defective uterine patterning along the dorsal-ventral axis in the ablation group. (A and B) Representative images of DAPI staining of PND0 uteri in the control and ablation groups. The mispatterning was observed throughout the entire uterine horn on PND0. (C and D) Histology of PND21 uteri in the control and ablation groups. The mispatterning in two of three PND21 uteri in the ablation group was resolved. Dashed circles: uterine lumens. Scale bar: 100 μm. $N = 6$, 5, 4, 3 for A, B, C, D, respectively.

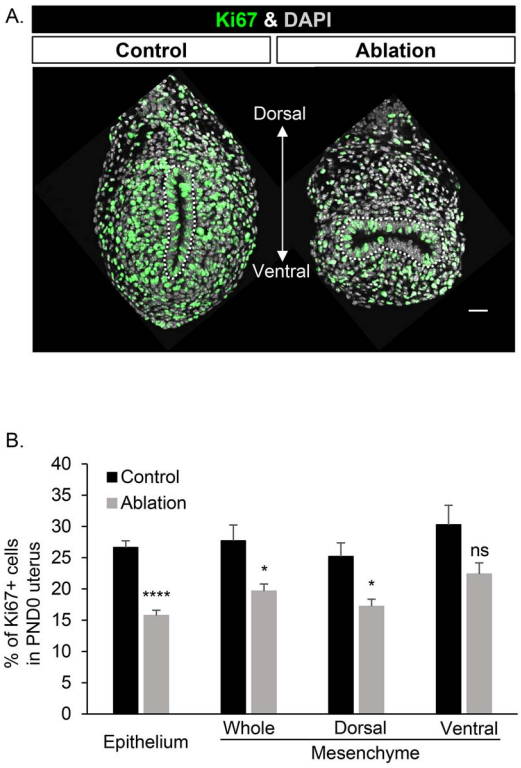

Figure 8. Decreased cell proliferation in epithelial and mesenchymal compartments of the uterus in the ablation group. (A) Representative images of Ki67 immunofluorescence staining on PND0 uteri of the control and ablation groups. Nuclei were stained with DAPI. White dashed circles: uterine lumen. Scale bar: 25 μm. (B) Percentages of Ki67+ cells in the epithelial and mesenchymal compartments of PND0 uteri in the control and ablation groups. $N = 4$–5. Results were shown as mean ± s.e.m. and analyzed by two-tailed unpaired Student's *t* test. ns, $P > 0.05$, not significant; *, $P < 0.05$; ****, $P < 0.0001$.

a specific cell type/lineage in development and function of the female reproductive tract.

Amhr2+ mesenchyme is essential for oviductal coiling

Tissue recombination studies have demonstrated that the mesenchyme plays inductive roles in epithelial region-specific

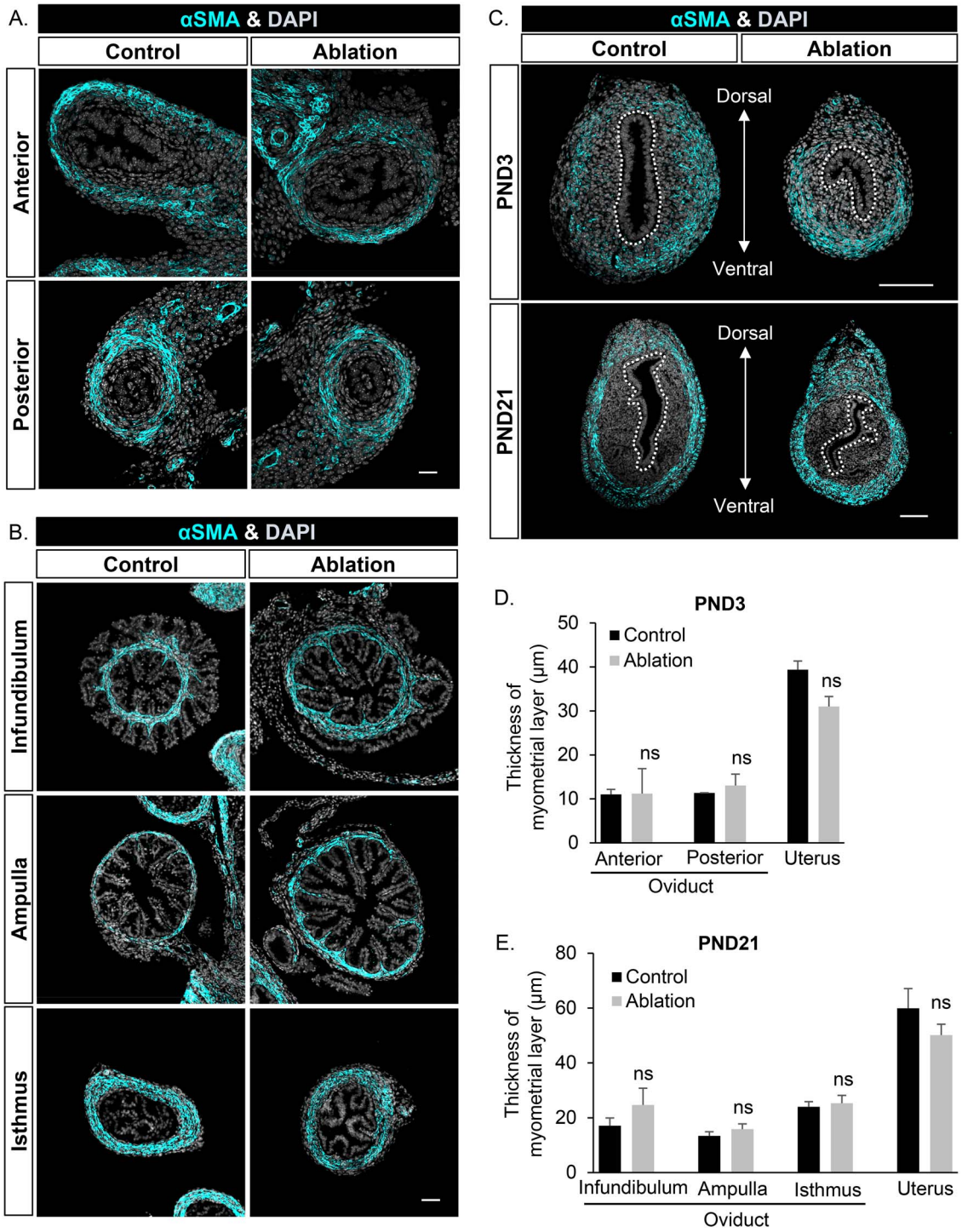

Figure 9. Delayed smooth muscle formation at the dorsal side of the uterus in the ablation group. (A–C) Representative images of αSMA immunofluorescence staining on PND3 oviducts (A), PND21 oviducts (B), and PND3 and PND21 uteri (C). $N = 3$–4. Scale bar: 100 μm. White dashed circles in C: uterine lumen. (D and E) Quantifications of thickness of myometrial layers in oviducts and uteri on PND3 (D) and PND21 (E). $N = 3$–7. Results were shown as mean ± s.e.m. and analyzed by two-tailed unpaired Student's *t* test. ns, $P > 0.05$, not significant compared to the control group at the same age.

fates and morphogenesis [3]. However, it is unknown which mesenchymal population directs oviductal epithelial morphogenesis. Using in vivo cellular ablation model, our study demonstrated the critical role of *Amhr2*+ mesenchyme in regulating epithelial proliferation, oviductal elongation and coiling during the antero-posterior patterning. Gene knockout mouse studies have showed that the function of mesenchyme in promoting oviductal coiling is highly dependent upon mesenchyme-derived growth factors. For example, WNT4 is a Wnt ligand that is specifically expressed in the mesonephric mesenchyme at the fetal stage [55]. Mice with partial loss of WNT4 function presented less-coiled oviducts on E18.5 [55].

Interestingly, the distribution pattern of secretory and ciliated cells along the antero-posterior axis of the oviduct was

not altered after the partial ablation of *Amhr2*+ mesenchyme. Tissue recombination studies have demonstrated that differentiation of oviductal epithelia into secretory or ciliated epithelial cells is dictated by geographically and functionally distinct oviductal mesenchymes [56]. For instance, when recombined with the mesenchyme of the ampulla regions, the epithelia of the isthmus exhibit the distribution pattern of secretory and ciliated cells observed in the ampulla region [56]. The normal distribution of the two major epithelial cell types in the oviduct in our cell ablation model suggests that partial ablation of *Amhr2*+ mesenchyme does not affect the abilities of region-specific mesenchyme in determining the undifferentiated epithelium to cilial and secretory epithelial type.

Amhr2+ mesenchyme directs uterine lumen patterning along the dorsal-ventral axis

Although *Amhr2*+ mesenchyme is a commonly targeted cell population in studying uterine biology, its functions in female reproductive tract development are still not fully understood. Conditional deletion of *Ctnnb1* [57, 58] or *Dicer* [59] in the *Amhr2*+ mesenchyme caused hypoplastic uteri as seen in our *Amhr2-Cre; Rosa-DTA* cellular ablation model. However, these tissue-specific gene knockout mice did not show the alteration in the direction of the long axis of uterine lumen. Therefore, our cellular ablation model not only confirms the essential role of *Amhr2*+ mesenchyme for cellular proliferation and tissue growth during Müllerian duct development, but also reveals a novel function of *Amhr2*+ mesenchyme in directing the long axis of uterine lumen. Smooth muscle is known to produce mechanical forces, which is critical for patterning lumen shape [60, 61]. In the ablation group, the delayed smooth muscle differentiation at the dorsal side might reduce mechanical force from the dorsal side for driving/maintaining the direction of the long axis of lumen shape in the dorsal-ventral axis.

AMHR2 is the specific receptor for mediating the action of AMH [1]. AMHR2 is expressed in the subluminal mesenchyme from E12.5 through PND6. However, its ligand AMH is not expressed in embryonic and neonatal ovaries until PND6 in mice [62] or PND4-6 in rats [63]. Due to the absence of AMH, AMH/AMHR2 signaling remains dormant in the female reproductive tract. Ectopic activation of AMHR2 by exogenous AMH treatment on PND1 via viral gene delivery caused uterine hypoplasia and failure of uterine gland formation [11], which are different phenotypes from those observed in our study (altered direction of the long axis of lumen shape and unaffected uterine gland formation). The phenotypes upon exogenous AMH treatment in their study could result from epithelial death because mesenchymal AMH/AMHR2 signaling is known to induce epithelial degeneration [1]. On the other hand, *Amhr2-Cre; Rosa-DTA* cellular ablation model in our study specifically targeted and ablated *Amhr2*+ mesenchymal cells. Therefore, varied phenotypes between these two studies can result from ablating different cell types.

Of note, during embryo implantation, the lumen shape forms a slit-like structure with its long axis in the dorsal-ventral direction, which must be in alignment with the future embryonic axis for establishing successful implantation. Postnatal deletion of *Rbpj* (the nuclear transducer of Notch signaling) in the whole uterus caused tilting of this lumen axis in the Notch pathway-independent manner, resulting in deflected uterine-embryonic axis and substantial embryo loss [64]. These results demonstrate the importance of proper establishment of lumen shape orientation and suggest that the uterus with abnormal direction of the long axis in the ablation group could not be able to support successful implantation.

In conclusion, we showed that partial ablation of *Amhr2*+ mesenchyme from the fetal stage impairs female reproductive tract patterning along both antero-posterior and dorsal-ventral axes. The oviduct lost its characteristic coiling due to decreased epithelial proliferation and oviductal elongation. Uterine lumen displayed abnormal shape with its long axis oriented in the left–right direction, perpendicular to the dorsal-ventral axis in the normal condition. Our work opens up the application of genetic cell ablation models for a greater understanding of the function of a specific cell lineage in female reproductive tract development.

Supplementary material

Supplementary material is available at *BIOLRE* online.

Data and materials availability

All data are available in the main text or the supplementary materials upon reasonable request.

Authors' contributions

S.J. and F.Z. conceived the study; F.Z. supervised the project; S.J. performed all experiments and analyzed the data. J.W. and M.C. analyzed the data. S.J. and F.Z. wrote the manuscript. All authors read and approved the final manuscript.

Acknowledgments

We are thankful to Animal Care Staff in the School of Veterinary Medicine for taking care of our mouse colonies.

Conflict of interest

Authors declare that they have no competing interests.

References

1. Mullen RD, Behringer RR. Molecular genetics of Mullerian duct formation, regression and differentiation. *Sex Dev* 2014; **8**: 281–296.
2. Kurita T. Normal and abnormal epithelial differentiation in the female reproductive tract. *Differentiation* 2011; **82**:117–126.
3. Cunha GR. Stromal induction and specification of morphogenesis and cytodifferentiation of the epithelia of the Mullerian ducts and urogenital sinus during development of the uterus and vagina in mice. *J Exp Zool* 1976; **196**:361–369.
4. Dey SK, Lim H, Das SK, Reese J, Paria BC, Daikoku T, Wang H. Molecular cues to implantation. *Endocr Rev* 2004; **25**:341–373.
5. Vue Z, Gonzalez G, Stewart CA, Mehra S, Behringer RR. Volumetric imaging of the developing prepubertal mouse uterine epithelium using light sheet microscopy. *Mol Reprod Dev* 2018; **85**:397–405.
6. Vue Z, Behringer RR. Epithelial morphogenesis in the perinatal mouse uterus. *Dev Dyn* 2020; **249**:1377–1386.
7. Kelleher AM, DeMayo FJ, Spencer TE. Uterine glands: developmental biology and functional roles in pregnancy. *Endocr Rev* 2019; **40**:1424–1445.
8. Goad J, Ko YA, Kumar M, Syed SM, Tanwar PS. Differential Wnt signaling activity limits epithelial gland development to the

anti-mesometrial side of the mouse uterus. *Dev Biol* 2017; **423**: 138–151.
9. Kobayashi A, Stewart CA, Wang Y, Fujioka K, Thomas NC, Jamin SP, Behringer RR. β-Catenin is essential for Müllerian duct regression during male sexual differentiation. *Development* 2011; **138**:1967–1975.
10. Arango NA, Kobayashi A, Wang Y, Jamin SP, Lee HH, Orvis GD, Behringer RR. A mesenchymal perspective of Mullerian duct differentiation and regression in Amhr2-lacZ mice. *Mol Reprod Dev* 2008; **75**:1154–1162.
11. Saatcioglu HD, Kano M, Horn H, Zhang L, Samore W, Nagykery N, Meinsohn MC, Hyun M, Suliman R, Poulo J, Hsu J, Sacha C *et al.* Single-cell sequencing of neonatal uterus reveals an Misr2+ endometrial progenitor indispensable for fertility. *Elife* 2019; **8**:e46349. https://doi.org/10.7554/eLife.46349.
12. Huang CC, Orvis GD, Wang Y, Behringer RR. Stromal-to-epithelial transition during postpartum endometrial regeneration. *PLoS One* 2012; **7**:e44285.
13. Ni N, Fang X, Li Q. Functional similarity between TGF-beta type 2 and type 1 receptors in the female reproductive tract. *Sci Rep* 2021; **11**:9294.
14. Li Q, Agno JE, Edson MA, Nagaraja AK, Nagashima T, Matzuk MM. Transforming growth factor beta receptor type 1 is essential for female reproductive tract integrity and function. *PLoS Genet* 2011; **7**:e1002320.
15. St-Jean G, Tsoi M, Abedini A, Levasseur A, Rico C, Morin M, Djordjevic B, Miinalainen I, Kaarteenaho R, Paquet M, Gevry N, Boyer A *et al.* Lats1 and Lats2 are required for the maintenance of multipotency in the Mullerian duct mesenchyme. *Development* 2019; **146.**(20):dev180430.
16. Ivanova A, Signore M, Caro N, Greene ND, Copp AJ, Martinez-Barbera JP. In vivo genetic ablation by Cre-mediated expression of diphtheria toxin fragment A. *Genesis* 2005; **43**:129–135.
17. Jamin SP, Arango NA, Mishina Y, Hanks MC, Behringer RR. Requirement of Bmpr1a for Mullerian duct regression during male sexual development. *Nat Genet* 2002; **32**:408–410.
18. Li Q, Pangas SA, Jorgez CJ, Graff JM, Weinstein M, Matzuk MM. Redundant roles of SMAD2 and SMAD3 in ovarian granulosa cells in vivo. *Mol Cell Biol* 2008; **28**:7001–7011.
19. Zhao F, Li R, Xiao S, Diao H, Viveiros MM, Song X, Ye X. Post-weaning exposure to dietary zearalenone, a mycotoxin, promotes premature onset of puberty and disrupts early pregnancy events in female mice. *Toxicol Sci* 2013; **132**:431–442.
20. Zhao F, Franco HL, Rodriguez KF, Brown PR, Tsai MJ, Tsai SY, Yao HH. Elimination of the male reproductive tract in the female embryo is promoted by COUP-TFII in mice. *Science* 2017; **357**: 717–720.
21. Fayzullina S, Martin LJ. Detection and analysis of DNA damage in mouse skeletal muscle in situ using the TUNEL method. *J Vis Exp* 2014; (**94**):52211. https://doi.org/10.3791/52211.
22. Saadeh H, Abdullah N, Erashdi M, Sughayer M, Al-Kadi O. Histopathologist-level quantification of Ki-67 immunoexpression in gastroenteropancreatic neuroendocrine tumors using semiautomated method. *J Med Imaging (Bellingham)* 2020; **7**:012704.
23. Miller I, Min M, Yang C, Tian C, Gookin S, Carter D, Spencer SL. Ki67 is a graded rather than a binary marker of proliferation versus quiescence. *Cell Rep* 2018; **24**:1105–1112.e5.
24. Agduhr E. Studies on the structure and development of the bursa ovarica and the tuba uterina in the mouse. *Acta Zoologica* 1927; **8**:1–133.
25. Brockschnieder D, Lappe-Siefke C, Goebbels S, Boesl MR, Nave KA, Riethmacher D. Cell depletion due to diphtheria toxin fragment A after Cre-mediated recombination. *Mol Cell Biol* 2004; **24**: 7636–7642.
26. Huang CC, Orvis GD, Kwan KM, Behringer RR. Lhx1 is required in Mullerian duct epithelium for uterine development. *Dev Biol* 2014; **389**:124–136.
27. Stewart CA, Behringer RR. Mouse oviduct development. *Results Probl Cell Differ* 2012; **55**:247–262.
28. Ma L, Benson GV, Lim H, Dey SK, Maas RL. Abdominal B (AbdB) Hoxa genes: regulation in adult uterus by estrogen and progesterone and repression in mullerian duct by the synthetic estrogen diethylstilbestrol (DES). *Dev Biol* 1998; **197**:141–154.
29. D'Amours D, Sallmann FR, Dixit VM, Poirier GG. Gain-of-function of poly(ADP-ribose) polymerase-1 upon cleavage by apoptotic proteases: implications for apoptosis. *J Cell Sci* 2001; **114**:3771–3778.
30. Zhao F, Grimm SA, Jia S, Yao HH-C. Contribution of the Wolffian duct mesenchyme to the formation of the female reproductive tract. *PNAS Nexus* 2022; **1**(4):pgac182. https://doi.org/10.1093/pnasnexus/pgac182.
31. Cooke PS, Spencer TE, Bartol FF, Hayashi K. Uterine glands: development, function and experimental model systems. *Mol Hum Reprod* 2013; **19**:547–558.
32. Ruberte JS, Carretero A, Navarro M. *Morphological mouse phenotyping: anatomy, histology and imaging*. Amsterdam: Elsevier/Academic Press; 2017.
33. Barton BE, Herrera GG, Anamthathmakula P, Rock JK, Willie A, Harris EA, Takemaru KI, Winuthayanon W. Roles of steroid hormones in oviductal function. *Reproduction* 2020; **159**:R125–R137.
34. Yuan S, Wang Z, Peng H, Ward SM, Hennig GW, Zheng H, Yan W. Oviductal motile cilia are essential for oocyte pickup but dispensable for sperm and embryo transport. *Proc Natl Acad Sci U S A* 2021; **118**(22):e2102940118. https://doi.org/10.1073/pnas.2102940118.
35. Ford MJ, Harwalkar K, Pacis AS, Maunsell H, Wang YC, Badescu D, Teng K, Yamanaka N, Bouchard M, Ragoussis J, Yamanaka Y. Oviduct epithelial cells constitute two developmentally distinct lineages that are spatially separated along the distal-proximal axis. *Cell Rep* 2021; **36**:109677.
36. Ghosh A, Syed SM, Tanwar PS. In vivo genetic cell lineage tracing reveals that oviductal secretory cells self-renew and give rise to ciliated cells. *Development* 2017; **144**:3031–3041.
37. Jorgez CJ, Klysik M, Jamin SP, Behringer RR, Matzuk MM. Granulosa cell-specific inactivation of follistatin causes female fertility defects. *Mol Endocrinol* 2004; **18**:953–967.
38. Ogasawara Y, Okamoto S, Kitamura Y, Matsumoto K. Proliferative pattern of uterine cells from birth to adulthood in intact, neonatally castrated, and/or adrenalectomized mice, assayed by incorporation of [125I]iododeoxyuridine. *Endocrinology* 1983; **113**:582–587.
39. Luo XR, Ikeda YY, Parker KL. A cell-specific nuclear receptor is essential for adrenal and gonadal development and sexual-differentiation. *Cell* 1994; **77**:481–490.
40. Couse JF, Korach KS. Estrogen receptor null mice: what have we learned and where will they lead us? *Endocr Rev* 1999; **20**: 358–417.
41. Savin T, Kurpios NA, Shyer AE, Florescu P, Liang H, Mahadevan L, Tabin CJ. On the growth and form of the gut. *Nature* 2011; **476**: 57–62.
42. Andrew DJ, Ewald AJ. Morphogenesis of epithelial tubes: insights into tube formation, elongation, and elaboration. *Dev Biol* 2010; **341**:34–55.
43. Brody JR, Cunha GR. Histologic, morphometric, and immunocytochemical analysis of myometrial development in rats and mice: I. Normal development. *Am J Anat* 1989; **186**:1–20.
44. Gao Y, Bayless KJ, Li Q. TGFBR1 is required for mouse myometrial development. *Mol Endocrinol* 2014; **28**:380–394.
45. Jaslove JM, Nelson CM. Smooth muscle: a stiff sculptor of epithelial shapes. *Philos Trans R Soc Lond B Biol Sci* 2018; **373**:20170318.
46. Smith LB, O'Shaughnessy PJ, Rebourcet D. Cell-specific ablation in the testis: what have we learned? *Andrology* 2015; **3**: 1035–1049.
47. Shen YC, Shami AN, Moritz L, Larose H, Manske GL, Ma Q, Zheng X, Sukhwani M, Czerwinski M, Sultan C, Chen H, Gurczynski SJ *et al.* TCF21(+) mesenchymal cells contribute to testis

somatic cell development, homeostasis, and regeneration in mice. *Nat Commun* 2021; **12**:3876.
48. Caldeira-Brant AL, Eras-Garcia L, Alves-Freitas D, Almeida F, Chiarini-Garcia H. Spermatogonial behavior in marmoset: a new generation, their kinetics and niche. *Mol Hum Reprod* 2018; **24**: 299–309.
49. Turner EC, Hughes J, Wilson H, Clay M, Mylonas KJ, Kipari T, Duncan WC, Fraser HM. Conditional ablation of macrophages disrupts ovarian vasculature. *Reproduction* 2011; **141**:821–831.
50. Niu W, Spradling AC. Two distinct pathways of pregranulosa cell differentiation support follicle formation in the mouse ovary. *Proc Natl Acad Sci U S A* 2020; **117**:20015–20026.
51. Care AS, Diener KR, Jasper MJ, Brown HM, Ingman WV, Robertson SA. Macrophages regulate corpus luteum development during embryo implantation in mice. *J Clin Invest* 2013; **123**:3472–3487.
52. Mucenski ML, Mahoney R, Adam M, Potter AS, Potter SS. Single cell RNA-seq study of wild type and Hox9,10,11 mutant developing uterus. *Sci Rep* 2019; **9**:4557.
53. Kirkwood PM, Gibson DA, Smith JR, Wilson-Kanamori JR, Kelepouri O, Esnal-Zufiaurre A, Dobie R, Henderson NC, Saunders PTK. Single-cell RNA sequencing redefines the mesenchymal cell landscape of mouse endometrium. *FASEB J* 2021; **35**:e21285.
54. McGlade EA, Herrera GG, Stephens KK, Olsen SLW, Winuthayanon S, Guner J, Hewitt SC, Korach KS, DeMayo FJ, Lydon JP, Monsivais D, Winuthayanon W. Cell-type specific analysis of physiological action of estrogen in mouse oviducts. *FASEB J* 2021; **35**:e21563.
55. Prunskaite-Hyyrylainen R, Skovorodkin I, Xu Q, Miinalainen I, Shan J, Vainio SJ. Wnt4 coordinates directional cell migration and extension of the Mullerian duct essential for ontogenesis of the female reproductive tract. *Hum Mol Genet* 2016; **25**:1059–1073.
56. Yamanouchi H, Umezu T, Tomooka Y. Reconstruction of oviduct and demonstration of epithelial fate determination in mice. *Biol Reprod* 2010; **82**:528–533.
57. Deutscher E, Hung-Chang YH. Essential roles of mesenchyme-derived beta-catenin in mouse Mullerian duct morphogenesis. *Dev Biol* 2007; **307**:227–236.
58. Hernandez Gifford JA, Hunzicker-Dunn ME, Nilson JH. Conditional deletion of beta-catenin mediated by Amhr2cre in mice causes female infertility. *Biol Reprod* 2009; **80**:1282–1292.
59. Gonzalez G, Behringer RR. Dicer is required for female reproductive tract development and fertility in the mouse. *Mol Reprod Dev* 2009; **76**:678–688.
60. Heisenberg CP, Bellaiche Y. Forces in tissue morphogenesis and patterning. *Cell* 2013; **153**:948–962.
61. Hinz B. The myofibroblast: paradigm for a mechanically active cell. *J Biomech* 2010; **43**:146–155.
62. Munsterberg A, Lovell-Badge R. Expression of the mouse anti-Mullerian hormone gene suggests a role in both male and female sexual differentiation. *Development* 1991; **113**:613–624.
63. Ueno S, Takahashi M, Manganaro TF, Ragin RC, Donahoe PK. Cellular localization of mullerian inhibiting substance in the developing rat ovary. *Endocrinology* 1989; **124**:1000–1006.
64. Zhang S, Kong S, Wang B, Cheng X, Chen Y, Wu W, Wang Q, Shi J, Zhang Y, Wang S, Lu J, Lydon JP *et al.* Uterine Rbpj is required for embryonic-uterine orientation and decidual remodeling via Notch pathway-independent and -dependent mechanisms. *Cell Res* 2014; **24**:925–942.